

Self-Attentive Spatio-Temporal Calibration for Precise Intermediate Layer Matching in ANN-to-SNN Distillation

Di Hong^{1,2,3}, Yueming Wang^{1,2,3*}

¹The College of Computer Science and Technology, Zhejiang University, China

²Nanhu Brain-computer Interface Institute, Hangzhou, China

³The State Key Laboratory of Brain-Machine Intelligence, Zhejiang University, China
{hongd, ymingwang} @zju.edu.cn

Abstract

Spiking Neural Networks (SNNs) are promising for low-power computation due to their event-driven mechanism but often suffer from lower accuracy compared to Artificial Neural Networks (ANNs). ANN-to-SNN knowledge distillation can improve SNN performance, but previous methods either focus solely on label information, missing valuable intermediate layer features, or use a layer-wise approach that neglects spatial and temporal semantic inconsistencies, leading to performance degradation. To address these limitations, we propose a novel method called *self-attentive spatio-temporal calibration* (*SASTC*). *SASTC* uses self-attention to identify semantically aligned layer pairs between ANN and SNN, both spatially and temporally. This enables the autonomous transfer of relevant semantic information. Extensive experiments show that *SASTC* outperforms existing methods, effectively solving the mismatching problem. Superior accuracy results include 95.12% on CIFAR-10, 79.40% on CIFAR-100 with 2 time steps, and 68.69% on ImageNet with 4 time steps for static datasets, and 97.92% on DVS-Gesture and 83.60% on DVS-CIFAR10 for neuromorphic datasets. This marks the first time SNNs have outperformed ANNs on both CIFAR-10 and CIFAR-100, shedding the new light on the potential applications of SNNs.

Code — <https://github.com/ieveresthd/SASTC.git>

Introduction

Spiking Neural Networks (SNNs), considered the third generation of neural networks (Maass 1997), offer a promising advancement in low-power computing. Unlike artificial neural networks (ANNs), which use continuous-valued activations, SNNs emulate the brain's discrete, spike-based information transmission, making them ideal for event-driven and energy-efficient neuromorphic hardware (Akopyan et al. 2015). Two main approaches have emerged for developing supervised deep SNNs: 1) direct training from scratch using surrogate gradients to approximate the discontinuous derivatives of spiking neurons, and 2) ANN-to-SNN conversion, which aligns ANN neuron functions with spiking neurons. Despite progress, a performance gap persists between ANNs

and SNNs. To address this, ANN-to-SNN knowledge distillation has been employed to transfer relevant knowledge from ANNs to SNNs.

However, previous distillation methods have either failed to transfer sufficient knowledge or have faced spatial and temporal disparities in semantic information, resulting in degraded performance. This paper introduces a Self-Attentive mechanism to address the semantic mismatch problem by autonomously identifying the most relevant semantic layer patterns across spatial and temporal dimensions and allocating attention based on semantic relevance. The key contributions of this work are summarized as follows:

1. We propose a self-attention mechanism to address semantic mismatching during ANN-to-SNN knowledge distillation by autonomously aligning the most relevant layer patterns between ANN and SNN both spatially and temporally.
2. Through extensive experiments across various settings and prevalent network architectures, our method significantly boosts SNN performance in ANN-to-SNN distillation, surpassing current benchmarks across various datasets, including both static and neuromorphic ones.
3. Our analysis demonstrates that *SASTC* successfully achieves semantic matching in ANN-to-SNN distillation, advancing its applications in robust representation.

Related Work

Direct Training from Scratch

We briefly summarize some significant achievements in direct training. Lee et al. directly train SNNs in terms of spikes by regarding the membrane potential as the combination of differentiable signals and discontinuous noisy (Lee, Delbrück, and Pfeiffer 2016). Wu et al. use an approximate derivative to construct an iterative LIF neuron model and propose a spatio-temporal backpropagation (STBP) method to train SNNs from scratch (Wu et al. 2018). Zheng et al. propose a threshold-dependent batch normalization (tdBN) method for tuning the loss function (Zheng et al. 2021). Rathi et al. propose to optimize the leakage and threshold in the LIF neuron model. Furthermore, many direct training method have been proposed based on designing various surrogate gradients and coding schemes to achieve SNNs with low latency and high performance (Wu et al. 2019).

*corresponding author.

Copyright © 2025, Association for the Advancement of Artificial Intelligence (www.aaai.org). All rights reserved.

ANN-to-SNN Conversion

Pérez-Carrasco et al. first map sigmoid neuron model of ANNs into LIF neuron model by utilizing scaling factor, which is determined according to neuron parameters and modified manually (Pérez-Carrasco et al. 2013). Diehl et al. propose to regulate firing rates of SNNs through weight normalization (Diehl et al. 2015). Cao et al. adopt only one hyperparameter, which is the firing threshold of spiking neurons, to approximate the rectified linear unit (ReLU) function of ANNs (Cao, Chen, and Khosla 2015). Based on the great success achieved in previous conversion schemes, many subsequent studies are devoted to minimizing various errors in conversion process (Sengupta et al. 2019).

ANN-to-SNN Distillation

Typically, SNNs employ the spike frequency of the output layer or the average membrane potential increment as inference indicators. Analogous to ANN distillation, the conventional ANN-to-SNN knowledge distillation minimizes the Kullback-Leibler (KL) divergence between these SNN inference indicators and the predictive class probability distributions of ANNs (Lee et al. 2021). Recent efforts explore the transfer of enriched information from feature maps to enhance performance (Hong et al. 2023).

Self-Attentive Spatio-Temporal Calibration

Notations and Background

In this section, we provide a concise overview of fundamental concepts and establish necessary notations for subsequent illustration or clarity, the term "teacher model" denotes the ANN model, while the "student model" refers to the SNN model unless explicitly specified. Let $\mathcal{X} = \{x_i, y_i\}_i^n$ represent the training dataset consisting of n instances and N categories, with x_i as the input vector and y_i as the corresponding target in the form of a one-hot encoding vector. The number of output channels and spatial dimensions represented as c , h and w , respectively. For a mini-batch data of size b , the output of each SNN layer s_l at time step t is denoted as $f_{s_l}^t \in \mathbb{R}^{b \times c_{s_l} \times h_{s_l} \times w_{s_l}}$, where the superscript t signifies the index of the current time step, and T represents the total number of time steps. Simultaneously, the output of each ANN (teacher) layer a_l is denoted as $f_{a_l} \in \mathbb{R}^{b \times c_{a_l} \times h_{a_l} \times w_{a_l}}$. The layer indices s_l and a_l traverse from 1 to s_L and a_L , respectively. Notably, s_L and a_L typically differ due to the intrinsic heterogeneity inherent in the teacher and student models. The output representations at the penultimate layer of the teacher and student models are labeled as f_{a_L} and f_{s_L} . Furthermore, we define the feature pattern F as the set of outputs from intermediate feature layers. F_s^t represents the feature pattern of the student model at time step t , $F_s^t = \{f_{s_l}^t \mid \forall l \in [1, \dots, L]\}$, while F_a denotes the feature pattern of the teacher model, $F_a = \{f_{a_l} \mid \forall l \in [1, \dots, L]\}$. It is crucial to note that this collection is a permutation rather than a combination. In other words, multiple collections with the same intermediate layers but in different orders signify distinct feature patterns.

Concerning the student model, the outputs of the final layer $f_{end}(\cdot)$ are represented as the averaged membrane po-

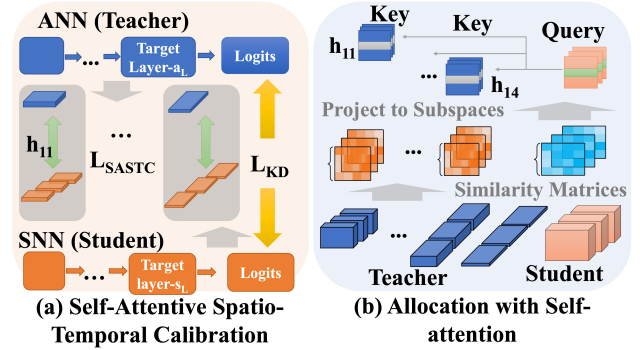


Figure 1: An overview of the proposed Self-Attentive Spatio-Temporal Calibration.

tentials over all time steps, $O_s^i = \frac{1}{T} \sum_{t=1}^T f_{end}(f_{s_L}^t[i]) \in \mathbb{R}^N$, where the notation i refers to the i -th input instance. We have added this clarification in the revised version. Predicted probabilities are derived through a softmax layer built on these outputs O_s^i , denoted as $P_s^i = \sigma(O_s^i/\alpha)$. Similarly, the logits of the teacher model are designated as $O_a^i = f_{end}(f_{a_L}[i]) \in \mathbb{R}^N$, and the corresponding predicted probabilities are denoted as $P_a^i = \sigma(O_a^i/\alpha)$, commonly referred to as soft targets. In both the student and teacher models, the hyperparameter α is typically set to 1.

Spatio-Temporal Mismatch Problem on Existing ANN-to-SNN Knowledge Distillation

Prior studies have assumed that: 1) the distributions of semantic information embedded in ANNs and SNNs are similar (spatially matched), and 2) this distribution within SNNs remains constant across different time steps (temporally matched). We introduce a metric named Spatio-Temporal Mismatch Score (STM score) to assess the extent of semantic disparity between associated ANN-SNN layer pairs over time steps. STM score is computed as the Average Euclidean Distance between the generated similarity matrices of each corresponding ANN-SNN feature map pair, as expressed in Equation (1):

$$STMscore = \frac{1}{T} \frac{1}{|C'|} \sum_{t=1}^T \sum_{C'} MSE(A_{s_l}^t, A_{a_l}). \quad (1)$$

where T represents the number of time steps, $|C'|$ denotes the number of candidate layer pairs, and $A_{s_l}^t$ and A_{a_l} are the similarity matrices of ANN layer a_l and SNN layer s_l , respectively. MSE measures the extent of semantic mismatches between the student SNN and the teacher ANN. A lower $STMscore$ signifies fewer mismatched association semantics, equating to superior model performance. Practically, we calculate the $STMscore$ (log-scale) values for each approach across training epochs and average them over the last 10 epochs, where they remain nearly unchanged.

Contrary to previous assumption, we find that existing ANN-to-SNN knowledge distillation methods either achieve

very small improvements or result in degradation effects on STM scores, as shown in Table 1. In other words, spatio-temporal mismatch of semantic information results in the loss of valuable knowledge during the knowledge distillation process. Our proposed approach diverges from the traditional paradigm by introducing self-attentive calibration. This innovative method aims to effectively transfer spatio-temporal semantic information by dynamically selecting suitable layer associations at each time step, departing from dependence on fixed teacher-student feature patterns.

SNN	Dataset	Time Step	STM score (↓)		
			Baseline	KD	FT
VGG-11	CIFAR-100	3	16.58	16.49	16.46
ResNet-18	CIFAR-100	3	16.97	16.85	16.73
ResNet-18	ImageNet	4	22.81	22.97	22.68

Note: teacher ANNs for CIFAR-100 and ImageNet are ResNet-32x4 and ResNet-34, respectively. The symbol (↓) indicates the smaller the better.

Table 1: Evaluation of Spatio-Temporal Mismatch Score on CIFAR-100 and ImageNet

Formulation of Self-Attentive Calibration

In our methodology, each student layer at every time step seamlessly aligns itself with semantically matched target layers through attention allocation, as depicted in Figure 1 (a) and (b). The training process, guided by calibrated associations, prompts the student model to adeptly gather and integrate information from multiple layers at each time step, fostering a more tailored regularization. Furthermore, SASTC is versatile and can be applied in scenarios where the number of candidate layers differs between the teacher and student models. The ensemble of acquired feature patterns at time step t in SASTC is denoted as $C^t = \{(f_{s_l}^t, f_{a_l}) \mid \forall f_{s_l}^t \in F_s^t, f_{a_l} \in F_a\}$, with the corresponding weight satisfying $\sum_{a_l=1}^{a_L} \eta_{(f_{s_l}^t, f_{a_l})}^t = 1, \forall f_{s_l}^t \in F_s^t$ at each time step. This weight $\eta_{(f_{s_l}^t, f_{a_l})}^t \in \mathbb{R}^{b \times T}$ signifies the degree to which the target layer f_{a_l} is considered in the calibration of spatio-temporal semantic differences during ANN-to-SNN distillation. A more detailed exploration of these self-attentive weights will be provided subsequently. The feature maps from each time step of the student model are transformed into a_L distinct forms, aligning with the spatial dimensions of each target layer for subsequent distance calculations, as indicated by

$$\hat{f}_{s_l, a_l}^t = \text{Proj}(f_{s_l}^t \in \mathbb{R}^{b \times c_{s_l} \times h_{s_l} \times w_{s_l}}, a_l), \quad (2)$$

$$f_{s_l}^t \in F_s^t, a_l \in [1, \dots, a_L],$$

with $\hat{f}_{s_l, a_l}^t \in \mathbb{R}^{b \times c_{a_l} \times h_{a_l} \times w_{a_l}}$. Each function $\text{Proj}(\cdot, \cdot)$ comprises a stack of two convolution layers with 3×3 and 1×1 to fulfill the requirement for an efficient transformation. This design choice is guided by previous research, which has illustrated the remarkable effectiveness of a 3×3 convolution layer and the pyramid architecture (Han, Kim, and Kim 2017).

Allocation with Self-attention Previous research suggests that the abstraction of feature representations is closely associated with the layer depth (Bengio, Courville, and Vincent 2013). The semantic levels of these intermediates can vary between teacher and student architectures with differing capacities. Furthermore, we observe variations in the semantic level among the feature patterns of SNNs at different time steps, resulting in spatio-temporal information loss during distillation. To address these spatio-temporal differences in the student model and enhance the performance of feature transfer during distillation, each layer of the student model should be associated with the most semantically relevant target layer to derive its own regularization. Simple approaches such as random selection or forcing feature maps from the same layer depths to align may be inadequate due to the adverse effects resulting from semantic mismatched pairs.

Inspired by the layer associations facilitated by attention mechanisms in ANNs (Vaswani et al. 2017), we expand the self-attentive scheme from spatial calibration to spatio-temporal calibration. This extension presents a potentially viable solution for addressing the semantic mismatch problem and enhancing the overall distillation performance. Given that feature maps in SNNs, generated by similar instances, tend to cluster at distinct granularities across different time steps and layers, and similarly, in ANNs, these feature maps cluster based on their depth, the proximity of pairwise similarity matrices serves as a meaningful measure of inherent semantic similarity. These similarity matrices are computed as follows

$$A_{s_l}^t = R(f_{s_l}^t) \cdot R(f_{s_l}^t)', \quad f_{s_l}^t \in F_s^t, \quad (3)$$

$$A_{a_l} = R(f_{a_l}) \cdot R(f_{a_l})', \quad f_{a_l} \in F_a,$$

where $R(\cdot) : \mathbb{R}^{b \times c \times h \times w} \rightarrow \mathbb{R}^{b \times c \times h \times w}$ represents a reshaping operation, and the symbol ' denotes the transpose operation. Consequently, $A_{s_l}^t$ and A_{a_l} yield $b \times b$ matrices. More importantly, incorporating similarity matrices significantly mitigates the memory cost associated with large spatio-temporal dimensions ($T \cdot c_{s_l/a_l} \cdot h_{s_l/a_l} \cdot w_{s_l/a_l} \gg b$).

Building upon the self-attention framework (Vaswani et al. 2017), we independently project the pairwise similarity matrices of each student layer, originating from individual time steps, and each target layer, into two subspaces using a Multi-Layer Perceptron (MLP). This procedure endeavors to alleviate the influence of noise and sparsity, with the resulting vectors identified as *query* and *key*. To expound further, for the i -th instance, the formulation can be articulated as follows:

$$Q_{s_l}^t[i] = \text{MLP}_Q(A_{s_l}^t[i]), \quad K_{a_l}[i] = \text{MLP}_K(A_{a_l}[i]). \quad (4)$$

The parameters in $\text{MLP}_Q(\cdot)$ and $\text{MLP}_K(\cdot)$ are acquired through training to produce *query* and *key* vectors, shared across all instances. Subsequently, the calibrated weight $\eta_{(f_{s_l}^t, f_{a_l})}^{t,i}$ for the i -th instance is computed as follows:

$$\eta_{(f_{s_l}^t, f_{a_l})}^{t,i} = \frac{e^{Q_{s_l}^t[i]' K_{a_l}[i]}}{\sum_{j=1}^{a_L} e^{Q_{s_l}^t[i]' K_j[i]}}. \quad (5)$$

The allocation based on attention offers a viable approach to alleviate the adverse effects stemming from spatio-temporal differences (mismatch in student-teacher layer

pairs) and amalgamate beneficial guidance from multiple target layers. The complete training procedure, incorporating the proposed semantic calibration formulation, is succinctly outlined in Algorithm 1.

Loss Function In a mini-batch of size b , the student model generates multiple feature patterns spanning various time steps (F_s^t, \dots, F_s^T). Following dimensional projections and self-attentive calibration, we employ Mean-Square-Error (MSE) to align the raw pairwise similarity matrices of the teacher and student (referred to as the loss of SASTC),

$$\begin{aligned}\mathcal{L}_{SASTC} &= \sum_t \sum_l \eta_{(f_{s_l}^t, f_{a_l})}^t Dist(f_{a_l}, Proj(f_{s_l}^t, a_l)) \\ &= \sum_{i=1}^b \sum_{t=1}^T \sum_{a_l=1}^{a_L} \sum_{s_l=1}^{s_L} \eta_{(f_{s_l}^t, f_{a_l})}^{t,i} MSE(f_{a_l}[i], \hat{f}_{s_l, a_l}^t[i]),\end{aligned}\quad (6)$$

as it demonstrated superior empirical performance. In this process, each feature map from the student model $f_{s_l}^t$ undergoes transformation via a projection function $Trans_s = Proj(\cdot, \cdot)$, while the target layers remain unchanged through identity transformation $Trans_a(\cdot) = I(\cdot)$. Multiplying the outcomes by the learned self-attentive distributions, the total loss is computed through a weighted summation of individual distances among feature maps from candidate teacher-student layer pairs at each time step. Consequently, the total loss of SASTC is expressed as:

$$\mathcal{L}_{total} = \mathcal{L}_{KD} + \beta \mathcal{L}_{SASTC}. \quad (7)$$

$$\mathcal{L}_{KD} = \mathcal{L}_{CE}(y_i, \sigma(O_s^i)) + \alpha^2 \mathcal{L}_{KL}\left(\frac{\sigma(O_a^i)}{\alpha}, \frac{\sigma(O_s^i)}{\alpha}\right). \quad (8)$$

where \mathcal{L}_{CE} represents the standard cross-entropy loss (CE) between the predicted probabilities of the student model and the one-hot target, and \mathcal{L}_{KL} denotes the KL divergence between P_s^i and the soft targets of the teacher model P_a^i .

Neuron Model and Surrogate Gradient

LIF Neuron We employ the LIF neuron model, which in discrete time, is described by:

$$u^t = \lambda u^{t-1} + I^t, \quad o^t = \Theta(u^t - V_{th}), \quad (9)$$

where u signifies the membrane potential, I^t denotes pre-synaptic inputs, $\lambda (< 1)$ represents the constant leaky factor in the membrane potential, V_{th} signifies the threshold membrane potential, Θ stands for the Heaviside step function, o denotes the spike output propagating to the next layer, and the superscript t indicates the time step. Following the emission of the spike output, the reset operation is delineated in

$$u^t = u^t \cdot (1 - o^t). \quad (10)$$

To minimize trainable parameters, all neurons share identical leak values λ and threshold potentials V_{th} . For consistency across experiments, we set the initial membrane potential u^0 to 0, the threshold V_{th} to 1, and the leaky factor λ to 0.5.

Algorithm 1: Self-Attentive Spatio-Temporal Calibration for ANN-to-SNN Knowledge Distillation

Input: Training dataset $X = (x_i, y_i)_{i=1}^n$; A pre-trained ANN (teacher model) with parameter \mathcal{W}^a ; An SNN (student model) with randomly initialized parameter \mathcal{W}^s ;

- 1: **while** \mathcal{W}^s is not converged **do**
- 2: Sample a mini-batch b size samples from X named \mathcal{B} .
- 3: Obtain intermediate layers' presentations \mathbf{F}_s^t across time steps and \mathbf{F}_a by propagating \mathcal{B} into \mathcal{W}^a and \mathcal{W}^s .
- 4: Construct pairwise similarity matrices $A_{s_l}^t$ and A_{a_l} as Equation (3).
- 5: Perform self-attention based spatio-temporal calibration as Equation (4-5).
- 6: Spatially align feature patterns across time steps as Equation (2).
- 7: Update parameters \mathcal{W}^s by propagating backward the surrogate gradients as defined in Equation (11) of the loss in Equation (7) and Equation (6).
- 8: **end while**

Triangle Shape Surrogate Gradient In this study, prioritizing a balance between accuracy and computational efficiency, we choose the triangular surrogate gradient, as established in prior research (Deng et al. 2022). The mathematical expression for the triangular surrogate gradient is as follows:

$$\frac{\partial o}{\partial u} = \frac{1}{\gamma^2} \max(0, \gamma - |u - V_{th}|), \quad (11)$$

with γ set to 0.3 based on previous works (Deng et al. 2022).

Experiments

To demonstrate the effectiveness of our proposed self-attentive spatio-temporal calibration in ANN-to-SNN knowledge distillation, we conduct comprehensive experiments. We evaluate various ANN-SNN combinations using popular network architectures like VGG (Simonyan and Zisserman 2014), ResNet (He et al. 2016), PyramidNet (Han, Kim, and Kim 2017), and WRN (Zagoruyko and Komodakis 2016) on static datasets. Meticulously designed experiments and ablation studies validate the effectiveness of SASTC in providing proper regularization for student models. We apply SASTC to neuromorphic datasets like DVS-Gesture and DVS-CIFAR10, demonstrating its robust generalization in noisy-label learning. Additionally, we offer a visual analysis of SASTC's success.

Further analyses of temporal information dynamics are provided in Appendix 1, with demonstrations of robust generalization of few-shot learning in Appendix 2. Details on batch size, sensitivity, computational efficiency, running time, and memory consumption are summarized in Appendix 3. The experimental setup details are available in Appendix 4.

SNN (student)	Baseline			ANN (teacher)	KD			Feature KD			SASTC		
	T=2	T=3	T=7		T=2	T=3	T=7	T=2	T=3	T=7	T=2	T=3	T=7
CIFAR-10													
VGG-11	92.48	92.80	93.16	ResNet-19	93.01	92.92	93.22	93.28	93.48	93.60	93.55	93.73	93.92
				Pyramidnet-20	92.98	93.07	93.52	93.04	93.28	93.36	93.52	93.70	93.64
				WRN-28-4	92.14	92.83	93.22	92.64	92.80	93.48	93.07	93.10	93.70
ResNet-18	94.04	94.12	94.72	WRN-28-4	94.24	94.44	94.68	94.92	95.44	95.76	95.12	95.24	95.48
				Pyramidnet-20	94.16	94.24	94.48	94.60	95.16	95.48	94.92	95.00	95.16
WRN-16-2	89.40	89.48	90.80	ResNet-19	92.36	92.52	93.36	92.16	93.13	93.26	94.12	94.16	94.12
				Pyramidnet-20	92.04	92.60	93.28	92.86	93.18	93.51	93.16	93.76	93.96
				WRN-28-4	91.72	92.20	92.92	92.16	93.08	93.44	93.16	93.28	93.72
CIFAR-100													
VGG-11	68.70	69.76	70.00	VGG-13	73.44	74.52	75.24	74.01	74.43	75.11	74.60	74.88	76.36
				ResNet-32x4	73.28	74.32	75.16	73.76	73.88	75.07	75.40	76.80	77.08
				WRN-40-2	74.24	75.16	75.48	74.31	75.07	75.48	74.48	75.60	75.72
ResNet-18	70.56	75.72	76.40	ResNet-32x4	77.68	78.00	78.64	77.01	77.96	78.09	80.28	80.24	80.68
				WRN-40-2	77.56	78.00	79.12	77.14	77.68	78.24	77.76	78.36	78.84

Note: baseline SNNs are trained from scratch using the same surrogate gradient as our distilled student models.

Table 2: Top-1 Test Accuracy(%) of Different ANN-to-SNN Distillation Approaches on CIFAR-10 and CIFAR-100 datasets

Comparison to Conventional ANN-to-SNN Distillation Methods

Top-1 test accuracy (%) on CIFAR-10 and CIFAR-100 across seventeen distinct ANN-SNN combinations is illustrated in Table 2. Four of these combinations share similar architectures (WRN-16-2/28-4, VGG-11/13, ResNet-18/32x4), while the remaining nine are heterogeneous. Since the large memory consumption of traditional feature ANN-to-SNN KD method , we train the student SNN with different single layer combination settings and calculate their average value as the final result (*i.e.*, Feature KD in Table 2).

Table 2 illustrates that SASTC demonstrates significant relative improvement across all compared methods on both CIFAR-10 and CIFAR-100 datasets, indicating its ability to effectively leverage intermediate information across time steps for superior distillation results. The most notable enhancements occur in the "WRN-16-2 & ResNet-19" (T=2) and the "ResNet-18 & ResNet-32x4" (T=2), with a 4.72% improvement over baseline on CIFAR-10 and a 8.84% improvement over baseline on CIFAR-100. Notably, when compared to the competitive distillation method feature KD, results with combinations of WRN-16-2/ResNet-19 on CIFAR-10 and all combinations on CIFAR-100 meet performance degradation phenomenon compared to the vanilla ANN-to-SNN KD method (the detailed explanation of these negative regularization effects is illustrated in the section of mechanism analysis).

Moreover, we achieve significant improvements on ImageNet, which is illustrated in Table 3. Despite training for only 90 epochs, SASTC improves ResNet-18 performance by 2.02% over the baseline SNN. Additionally, SASTC achieves 1.15% and 1.51% improvements over vanilla and feature-based ANN-to-SNN KD on ResNet-18, respectively. Notably, feature-based method shows significant negative

Method	Architecture	Time Steps	Accuracy
Baseline	ResNet-18	4	60.50
KD	ResNet-18	4	61.37
Feature KD	ResNet-18	4	61.01
SASTC	ResNet-18	4	62.52
	ResNet-34	4	68.69
Teacher (ANN)	ResNet-34	1	73.48

Table 3: Top-1 Test Accuracy(%) of ANN-to-SNN Distillation Approaches on ImageNet dataset

regularization effects during the ANN-to-SNN distillation process on ImageNet.

Comparison to Existing SNN Training Methods

In this section, we present a comparison of our experimental results with previous conventional training methods, summarized in Table 4.

On the CIFAR-10 dataset, our SASTC outperforms all existing approaches, achieving the highest accuracy and the lowest inference latency. Specifically, even with $T = 2$, there is 0.62% and 1.96% increments compared to advanced TET (Deng et al. 2022) and STBP-tdBn (Zheng et al. 2021) with $T=6$, respectively. On the CIFAR-100 dataset, SASTC consistently demonstrates superior performance and faster inference, surpassing STBP-tdBn (Zheng et al. 2021) by 9.56% to 9.99% and TET (Deng et al. 2022) by 4.68% to 5.96% across all reported time steps. Notably, our method first outperforms the ANN counterpart with the spatio-temporal calibration on both CIFAR-10 and CIFAR-100, the relatively maximum increments are 0.51% and 5.33%, respectively.

On the ImageNet dataset, the SASTC algorithm achieves a 3.90% increment compared to TET (Deng et al. 2022) with smaller 4 time steps. Although SEW-ResNet34 devi-

ates from a typical SNN as it adopts the IF model and modifies the Residual structure, SASTC achieves 1.65% improvement than SEW-ResNet (Fang et al. 2021)

Dataset	Method	Architecture	Time	Steps	Accuracy
CIFAR-10	Norm (Sengupta et al. 2019)	VGG-16	2500	91.55	
	Norm (Han, Srinivasan, and Roy 2020)	VGG-16	2048	93.63	
	Norm (Deng and Gu 2021)	VGG-16	16	92.29	
	STBP (Wu et al. 2018)	CIFARNet	12	89.83	
	STBP NeuNorm (Wu et al. 2019)	CIFARNet	12	90.53	
	Hybrid (Rathi et al. 2020)	ResNet-20	250	92.22	
	DIET-SNN (Rathi and Roy 2021)	ResNet-20	10	92.54	
	TET (Deng et al. 2022)	ResNet-19	6	94.50	
	TSSL-BP (Zhang and Li 2020)	CIFARNet	5	91.41	
	STBP-tdBn (Zheng et al. 2021)	ResNet-19	6	93.16	
CIFAR-100	GLIF (Yao et al. 2022)	ResNet-19	2	94.44	
	KDSNN (Xu et al. 2023)	VGG-16	4	91.05	
	Norm (Bu et al. 2023)	VGG-16	4	93.96	
	TKS (Dong, Zhao, and Zeng 2024)	ResNet-19	4	95.30	
	SSCL-SNN (Zhang et al. 2024)	ResNet-20	4	94.27	
	Ours	ResNet-18	7	95.48	
			3	95.24	
			2	95.12	
	ANN (Deng et al. 2022)	ResNet-19	1	94.97	
	Hybrid (Rathi et al. 2020)	VGG-11	125	67.87	
ImageNet	DIET-SNN (Rathi and Roy 2021)	VGG-16	5	69.67	
	TET (Deng et al. 2022)	ResNet-19	6	74.72	
			6	71.12	
	STBP-tdBn (Zheng et al. 2021)	ResNet-19	4	70.86	
			2	69.41	
	GLIF (Yao et al. 2022)	ResNet-19	2	75.48	
	Norm (Bu et al. 2023)	VGG-16	4	69.62	
	TKS (Dong, Zhao, and Zeng 2024)	ResNet-19	4	76.20	
	SSCL-SNN (Zhang et al. 2024)	ResNet-19	2	78.79	
	Ours	ResNet-18	7	80.68	
			3	80.24	
			2	80.28	
	ANN (Deng et al. 2022)	ResNet-19	1	75.35	
	Hybrid (Rathi et al. 2020)	ResNet-34	250	61.48	
	SPIKE-NORM (Sengupta et al. 2019)	ResNet-34	2500	69.96	
	STBP-tdBn (Zheng et al. 2021)	Spiking-ResNet-34	6	63.72	
	SEW ResNet (Fang et al. 2021)	SEW-ResNet-34	4	67.04	
	TET (Deng et al. 2022)	Spiking-ResNet-34	6	64.79	
	SSCL-SNN (Zhang et al. 2024)	ResNet-34	4	66.78	
	MS-ResNet (Hu et al. 2024)	ResNet-18	6	63.10	
	Ours	ResNet-18	4	62.52	
		ResNet-34	4	68.69	

Table 4: Top-1 Test Accuracy(%) of Different SNN Methods on Static Datasets

Mechanism Analysis and Ablation Study

In this section, we delve into an experimental exploration of the negative regularization effect induced by manually specified layer associations across time steps. Furthermore, we provide evidence of the success of SASTC, supported by the proposed criterion and visual evidence.

SASTC Improves Negative Regularization Effects We conduct experiments on the CIFAR-10 dataset by training the student model exclusively with a specified teacher-student layer pair in various settings, and observe negative regularization effects that feature-pattern-based distillation with specific layer associations across time steps performs worse than vanilla ANN-to-SNN KD. The network architectures involved "VGG-11& ResNet-19", "ResNet-18 & Pyramidnet-20", and "WRN-16-2 & WRN-28-4". The numbers of candidate target layers and student layers for each case are (4, 5), (3, 4), and (4, 4), respectively.

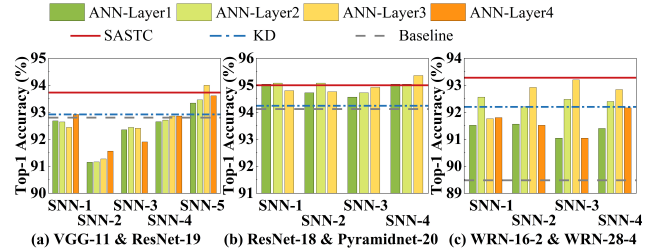


Figure 2: Illustration of negative regularization on CIFAR-10 with three model combinations. Each tick label of x-axis denotes an SNN (student) layer number. Different color bars indicate the results of different specified ANN-SNN layer combinations.

The outcomes of student models with 20, 12 and 16 ANN-SNN layer combinations under the three settings on CIFAR-10 are illustrated in Fig. 2. Notably, all layer associations of SNN layer-2 and layer-3 in Fig. 2 (a) obtain extremely poor performance, likely due to highly sparse semantic information contained in layer-2 of VGG-11 student model. In addition, the performance of a student model significantly diminishes for certain layer associations across time steps (i.e., negative regularization effect), including SNN layer-1 to layer-4 in Fig. 2 (a) and (c), most like due to the substantial semantic mismatch. Notably, it is observed that the one-to-one layer matching scheme is non-optimal because better results can be obtained by leveraging information from a target layer with different depth, such as "SNN layer-5 & ANN-layer3" in Fig. 2 (a), "SNN layer-4 & ANN-layer3" in Fig. 2 (b) and "SNN layer-2 & ANN-layer3" in Fig. 2 (c).

Although training with specific hand-crafted layer associations may outperform SASTC in isolated cases like "SNN layer-5 & ANN-layer3" in Fig. 2 (a) and "SNN layer-4 & ANN-layer3" in Fig. 2 (b), SASTC consistently performs well across a large number of associations. It is particularly noteworthy considering that the knowledge of the best layer association for each network combination is not available in advance. Furthermore, instances where training with SASTC is inferior to the best layer association suggest potential refinements in our association strategy.

SASTC Achieves Semantic Matching during Knowledge Distillation The results in Table 5 indicate that SASTC consistently attains the lowest spatio-temporal mismatch score throughout the training process compared to other approaches owing to our spatio-temporal calibration mechanism on both CIFAR-100 and ImageNet datasets.

Moreover, we provide evidence in Appendix 1 that SASTC optimizes the temporal information dynamics of SNNs, further illustrating the success and mechanism of our proposed method.

Extension, Application and Visual Analysis

Extension to Neuromorphic Datasets Previous works focus on utilizing complex architectures to tackle the challenging DVS-CIFAR10 task. However, these sophisticated models have failed to achieve satisfied perfor-

SNN	Dataset	Time Step	STM score (↓)			
			Baseline	KD	FT	SASTC
VGG-11	CIFAR-100	3	16.58	16.49	16.46	16.30
ResNet-18	CIFAR-100	3	16.97	16.85	16.73	16.11
ResNet-18	ImageNet	4	22.81	22.97	22.68	22.09

Note: teacher ANNs for CIFAR-100 and ImageNet are ResNet-32x4 and ResNet-34, respectively. The symbol (↓) indicates the smaller the better.

Table 5: Evaluation of Spatio-Temporal Mismatch Score on CIFAR-100 and ImageNet

mance and are susceptible to overfitting. Recently, a temporal efficient training approach has achieved the state-of-the-art accuracy with the streamlined VGGSNN architecture. In this paper, we conduct experiments on the DVS-Gesture and DVS-CIFAR10 datasets. As shown in Table 6, our proposed method outperform the contemporary best-performing methods, the accuracy of SASTC increase to 97.92% on DVS-Gesture and 83.60% on DVS-CIFAR10 through the calibration of spatio-temporal semantic mismatches during ANN-to-SNN distillation. Consequently, our SASTC method significantly improves the processing temporal information ability of SNNs on neuromorphic tasks.

Method	Architecture	Time Step Accuracy	
DVS-Gesture			
PLIF (Fang et al. 2021)	c128k3s1-BN-PLIF-MPk2s2*5-DPFC512-PLIF-DP-FC110-PLIF-APk10s10	20	97.57
STBP-tdBN (Zheng et al. 2021)	CIFARNet	40	96.87
SLAYER (Shrestha and Orchard 2018)	8 layers	25	93.64
Ours	ResNet-18	16	97.92
DVS-CIFAR10			
STBP-tdBN (Zheng et al. 2021)	ResNet-19	10	67.80
Streaming Rollout (Kugele et al. 2020)	DenseNet	10	66.80
Conv3D (Wu et al. 2021)	LIAF-Net	10	71.70
LIAF (Wu et al. 2021)	LIAF-Net	10	70.40
TET (Deng et al. 2022)	VGGSNN	10	83.17
SSCL-SNN (Zhang et al. 2024)	ResNet-19	10	80.00
Ours	VGGSNN	10	83.60

Table 6: Top-1 Test Accuracy(%) of Different SNN Methods on Neuromorphic Datasets

Application to Robust Representation In addition to evaluating the clean test set performance, we introduce noisy-label learning datasets by randomly perturbing 10%, 20%, 30%, 40%, and 50% of labels in training images. As shown in Table 7, training the lightweight SNN with SASTC extremely enhances its robustness compared to other ANN-to-SNN knowledge distillation approaches and the teacher ANN counterpart.

Visualization Analysis of SASTC To visually elucidate the advantages of SASTC, we randomly selected several images from ImageNet, and highlight regions deemed crucial

Percentage of Noisy Labels	0%	10%	20%	30%	40%	50%
Teacher	79.42%	76.51%	73.63%	70.57%	68.08%	64.27%
(ResNet-32x4)						
Baseline	69.76%	66.84%	64.00%	61.40%	59.84%	54.48%
KD	74.32%	73.64%	72.64%	72.36%	71.36%	70.80%
Feature KD	73.96%	63.68%	63.36%	63.24%	62.96%	61.84%
SASTC	77.08%	75.49%	74.77%	74.62%	74.32%	73.87%

Note: SNNs adopt three time steps.

Table 7: Noisy-Label Learning: Top-1 Test Accuracy(%) of "VGG-11 & ResNet-32x4" Combination on CIFAR-100

for predicting the respective labels by utilizing Spike Activation Map (SAM) (Kim and Panda 2021). As depicted in Figure 3, SASTC consistently centralizes class-discriminative regions and excels in capturing more semantically related information, resembling the teacher model, while the compared methods scatter them in the surroundings.

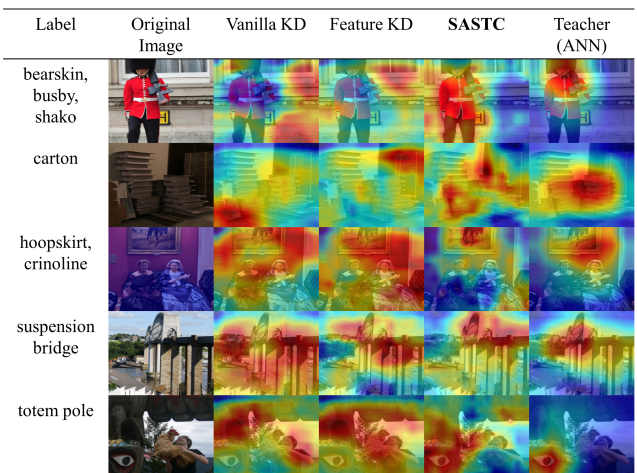


Figure 3: Spike Activation Map (SAM) visualization of ANN-to-SNN distillation approaches on ImageNet. The red regions highlight areas deemed important for model inference.

Conclusion

This study focuses on mitigating performance degradation due to spatio-temporal semantic mismatches and negative regularization in conventional ANN-to-SNN knowledge distillation methods. We propose a self-attentive mechanism to learn layer association weights across different time steps, enabling semantically aligned knowledge transfer. Qualitative and quantitative evidence validate SASTC's spatio-temporal calibration capability. Extensive experiments demonstrate that SASTC consistently outperforms various SNN training approaches and distillation schemes. SASTC also shows strong generalization across tasks and network architectures, excelling in robust representation.

Acknowledgments

This work was supported in part by the National Natural Science Foundation of China under Grants 62336007, in part by the Key R&D Program of Zhejiang under Grant 2022C03011, in part by the Starry Night Science Fund of Zhejiang University Shanghai Institute for Advanced Study under Grant SN-ZJU-SIAS-002, and in part by the Fundamental Research Funds for the Central Universities.

References

- Akopyan, F.; Sawada, J.; Cassidy, A.; Alvarez-Icaza, R.; Arthur, J.; Merolla, P.; Imam, N.; Nakamura, Y.; Datta, P.; Nam, G.-J.; Taba, B.; Beakes, M.; Brezzo, B.; Kuang, J. B.; Manohar, R.; Risk, W. P.; Jackson, B.; and Modha, D. S. 2015. TrueNorth: Design and Tool Flow of a 65 mW 1 Million Neuron Programmable Neurosynaptic Chip. *IEEE Transactions on Computer-Aided Design of Integrated Circuits and Systems*, 34(10): 1537–1557.
- Bengio, Y.; Courville, A.; and Vincent, P. 2013. Representation Learning: A Review and New Perspectives. *IEEE Transactions on Pattern Analysis and Machine Intelligence*, 35(8): 1798–1828.
- Bu, T.; Fang, W.; Ding, J.; Dai, P.; Yu, Z.; and Huang, T. 2023. Optimal ANN-SNN conversion for high-accuracy and ultra-low-latency spiking neural networks. *arXiv preprint arXiv:2303.04347*.
- Cao, Y.; Chen, Y.; and Khosla, D. 2015. Spiking deep convolutional neural networks for energy-efficient object recognition. *International Journal of Computer Vision*, 113: 54–66.
- Deng, S.; and Gu, S. 2021. Optimal conversion of conventional artificial neural networks to spiking neural networks. *arXiv preprint arXiv:2103.00476*.
- Deng, S.; Li, Y.; Zhang, S.; and Gu, S. 2022. Temporal efficient training of spiking neural network via gradient re-weighting. *arXiv preprint arXiv:2202.11946*.
- Diehl, P. U.; Neil, D.; Binas, J.; Cook, M.; Liu, S.-C.; and Pfeiffer, M. 2015. Fast-classifying, high-accuracy spiking deep networks through weight and threshold balancing. In *2015 International joint conference on neural networks (IJCNN)*, 1–8. iee.
- Dong, Y.; Zhao, D.; and Zeng, Y. 2024. Temporal Knowledge Sharing Enable Spiking Neural Network Learning From Past and Future . *IEEE Transactions on Artificial Intelligence*, 5(07): 3524–3534.
- Fang, W.; Yu, Z.; Chen, Y.; Masquelier, T.; Huang, T.; and Tian, Y. 2021. Incorporating learnable membrane time constant to enhance learning of spiking neural networks. In *Proceedings of the IEEE/CVF international conference on computer vision*, 2661–2671.
- Han, B.; Srinivasan, G.; and Roy, K. 2020. Rmp-snn: Residual membrane potential neuron for enabling deeper high-accuracy and low-latency spiking neural network. In *Proceedings of the IEEE/CVF conference on computer vision and pattern recognition*, 13558–13567.
- Han, D.; Kim, J.; and Kim, J. 2017. Deep pyramidal residual networks. In *Proceedings of the IEEE conference on computer vision and pattern recognition*, 5927–5935.
- He, K.; Zhang, X.; Ren, S.; and Sun, J. 2016. Deep residual learning for image recognition. In *Proceedings of the IEEE conference on computer vision and pattern recognition*, 770–778.
- Hong, D.; Shen, J.; Qi, Y.; and Wang, Y. 2023. LaSNN: Layer-wise ANN-to-SNN Distillation for Effective and Efficient Training in Deep Spiking Neural Networks. *arXiv preprint arXiv:2304.09101*.
- Hu, Y.; Deng, L.; Wu, Y.; Yao, M.; and Li, G. 2024. Advancing spiking neural networks toward deep residual learning. *IEEE Transactions on Neural Networks and Learning Systems*.
- Kim, Y.; and Panda, P. 2021. Visual explanations from spiking neural networks using inter-spike intervals. *Scientific reports*, 11(1): 1–14.
- Kugel, A.; Pfeil, T.; Pfeiffer, M.; and Chicca, E. 2020. Efficient processing of spatio-temporal data streams with spiking neural networks. *Frontiers in neuroscience*, 14: 512192.
- Lee, D.; Park, S.; Kim, J.; Doh, W.; and Yoon, S. 2021. Energy-efficient Knowledge Distillation for Spiking Neural Networks. *CoRR*, abs/2106.07172.
- Lee, J. H.; Delbrück, T.; and Pfeiffer, M. 2016. Training deep spiking neural networks using backpropagation. *Frontiers in neuroscience*, 10: 228000.
- Maass, W. 1997. Networks of spiking neurons: the third generation of neural network models. *Neural networks*, 10(9): 1659–1671.
- Pérez-Carrasco, J. A.; Zhao, B.; Serrano, C.; Acha, B.; Serrano-Gotarredona, T.; Chen, S.; and Linares-Barranco, B. 2013. Mapping from frame-driven to frame-free event-driven vision systems by low-rate rate coding and coincidence processing—application to feedforward ConvNets. *IEEE transactions on pattern analysis and machine intelligence*, 35(11): 2706–2719.
- Rathi, N.; and Roy, K. 2021. DIET-SNN: A low-latency spiking neural network with direct input encoding and leakage and threshold optimization. *IEEE Transactions on Neural Networks and Learning Systems*.
- Rathi, N.; Srinivasan, G.; Panda, P.; and Roy, K. 2020. Enabling deep spiking neural networks with hybrid conversion and spike timing dependent backpropagation. *arXiv preprint arXiv:2005.01807*.
- Sengupta, A.; Ye, Y.; Wang, R.; Liu, C.; and Roy, K. 2019. Going Deeper in Spiking Neural Networks: VGG and Residual Architectures. *Frontiers in Neuroscience*, 13.
- Shrestha, S. B.; and Orchard, G. 2018. Slayer: Spike layer error reassignment in time. *Advances in neural information processing systems*, 31.
- Simonyan, K.; and Zisserman, A. 2014. Very deep convolutional networks for large-scale image recognition. *arXiv preprint arXiv:1409.1556*.
- Vaswani, A.; Shazeer, N.; Parmar, N.; Uszkoreit, J.; Jones, L.; Gomez, A. N.; Kaiser, L.; and Polosukhin, I. 2017. Attention is all you need. *Advances in neural information processing systems*, 30.

- Wu, Y.; Deng, L.; Li, G.; and Shi, L. 2018. Spatio-temporal backpropagation for training high-performance spiking neural networks. *Frontiers in neuroscience*, 12: 323875.
- Wu, Y.; Deng, L.; Li, G.; Zhu, J.; Xie, Y.; and Shi, L. 2019. Direct training for spiking neural networks: Faster, larger, better. In *Proceedings of the AAAI Conference on Artificial Intelligence*, volume 33, 1311–1318.
- Wu, Z.; Zhang, H.; Lin, Y.; Li, G.; Wang, M.; and Tang, Y. 2021. Liaf-net: Leaky integrate and analog fire network for lightweight and efficient spatiotemporal information processing. *IEEE Transactions on Neural Networks and Learning Systems*, 33(11): 6249–6262.
- Xu, Q.; Li, Y.; Shen, J.; Liu, J. K.; Tang, H.; and Pan, G. 2023. Constructing deep spiking neural networks from artificial neural networks with knowledge distillation. In *Proceedings of the IEEE/CVF Conference on Computer Vision and Pattern Recognition*, 7886–7895.
- Yao, X.; Li, F.; Mo, Z.; and Cheng, J. 2022. Glif: A unified gated leaky integrate-and-fire neuron for spiking neural networks. *Advances in Neural Information Processing Systems*, 35: 32160–32171.
- Zagoruyko, S.; and Komodakis, N. 2016. Wide residual networks. *arXiv preprint arXiv:1605.07146*.
- Zhang, W.; and Li, P. 2020. Temporal spike sequence learning via backpropagation for deep spiking neural networks. *Advances in neural information processing systems*, 33: 12022–12033.
- Zhang, Y.; Liu, X.; Chen, Y.; Peng, W.; Guo, Y.; Huang, X.; and Ma, Z. 2024. Enhancing Representation of Spiking Neural Networks via Similarity-Sensitive Contrastive Learning. In *Proceedings of the AAAI Conference on Artificial Intelligence*, volume 38, 16926–16934.
- Zheng, H.; Wu, Y.; Deng, L.; Hu, Y.; and Li, G. 2021. Going deeper with directly-trained larger spiking neural networks. In *Proceedings of the AAAI conference on artificial intelligence*, volume 35, 11062–11070.

Appendix 1

SASTC Optimizes Temporal Information Dynamics of SNN

To quantify the Fisher information and further analysis its distribution of different ANN-to-SNN distillation methods, we introduce the empirical Fisher Information Matrix trace, denoted as FIM^t in Equation (1):

$$FIM^t = \frac{1}{n} \sum_{j=1}^n \|\nabla_w \log P_w(y|x_{k \leq t}^n)\|^2, \quad (1)$$

where k denotes the index of time step, and $P_w(y|x)$ denotes approximate posterior distribution of a network with weight parameters \mathcal{W} , input instance x from data distribution \mathcal{X} and output y .

In Fig. 1, we visualize temporal Fisher information of three different ANN-to-SNN distillation methods using the "VGG-11 & ResNet-19" combination on the CIFAR-10 dataset, along with the baseline as a reference. The Fisher information decreases notably with ANN-to-SNN distillation, and with training progression, the Fisher information with SASTC decreases more rapidly towards the final stable state compared to other distillation methods. In terms of temporal information distribution, ANN-to-SNN distillation can effectively supervise the optimization of the weight parameters, and our proposed SASTC is more effective than other ANN-to-SNN distillation methods.

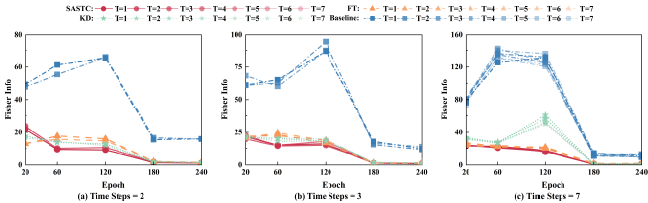


Figure 1: Illustration of temporal dynamics across training epochs of "VGG-11 & ResNet-19" combination on CIFAR-10. Four distinct colors represent three different distillation methods and the baseline model. Various levels of transparency within each color signify different time steps.

Application to Few-Shot Learning

Furthermore, we assess the performance of SASTC in few-shot learning and noisy-label learning scenarios. These experiments consistently demonstrate that SASTC effectively leverages training data and exhibits relative robustness to noisy perturbations.

We randomly select 25%, 50%, and 75% of training images from each class in CIFAR-100 to create several few-shot learning datasets. As depicted in Table 1, SASTC consistently outperforms the compared ANN-to-SNN distillation approaches and conventional training methods in all settings. The improvement becomes more significant as the number of available training images decreases. Notably, SASTC surpasses the teacher ANN counterpart and when trained with only 25% and 50% of the original dataset, which further prove the advantages of our SASTC.

Table 1: Few-Shot Learning: Top-1 Test Accuracy(%) of "VGG-11 & ResNet-32x4" Combination on CIFAR-100

Percentage of Training Images	25%	50%	75%	100%
Teacher (ResNet-32x4)	60.97%	70.87%	75.04%	79.42%
Baseline	46.48%	60.32%	66.76%	69.76%
KD	56.41%	66.94%	71.62%	74.32%
Feature KD	50.14%	57.97%	61.87%	73.96%
SASTC	66.19%	72.19%	74.44%	77.08%

Note: SNNs adopt three time steps.

Additional Analysis

Batch Size Analysis

We conduct experiments to analysis the influence of choosing different batch size in our proposed method, since our calculation of similarity matrices and self-attentive calibration is based on batch-level. To consider eliminating the impact of other factors, we introduce the vanilla ANN-to-SNN KD method for comparison as well as directly trained SNNs as the baseline. Results are summarized in Table 2. Although batch size is a crucial hyperparameter that influences training performance with the SGD optimizer (Keskar et al. 2016), the SNN obtained through SASTC consistently outperforms other SNNs in all cases.

Table 2: Impact of the Batch Size: Top-1 Test Accuracy(%) of "VGG-11 & ResNet-32x4" Combination on CIFAR-100

Batch Size	16	32	64	128	256
Baseline	72.96	73.52	73.48	73.24	72.44
KD	72.96	73.52	74.60	74.32	73.60
SASTC	74.56	75.80	76.4	76.36	76.24

Note: SNNs adopt three time steps.

Sensitivity Analysis

We evaluate the impact of the hyperparameter beta on the performance of SASTC across CIFAR-10 and CIFAR-100 datasets. Combinations of "VGG-11 & ResNet-19" with 3 time steps and "VGG-11 & ResNet-32x4" with 3 time steps are adopted on CIFAR-10 and CIFAR-100 respectively. Comparisons are made between SASTC with varying beta values, the vanilla ANN-to-SNN knowledge distillation approach (KD), and baseline SNNs. The hyperparameter β for SASTC ranges from 100 to 1500 at intervals of 100, while it remains 0 for KD, resulting in two horizontal lines in Fig. 2.

On the CIFAR-100 dataset, except for the β setting of 100, SASTC consistently outperforms both KD and the baseline in all other cases. Particularly, at the optimal hyperparameter setting ($\beta = 700$), SASTC exceeds KD and the baseline by 1.62 and 6.18 absolute accuracy, respectively. Similarly, on CIFAR-10, Fig. 2 demonstrates that SASTC consistently outperforms KD and the baseline across different β settings. At the optimal beta setting of 1300, our method surpasses KD and the baseline by 1.12 and 1.24 absolute accuracy, respectively. These findings demonstrate the effectiveness of our proposed method across a wide range of the β hyperparameter search space.

Comparison of Computation Efficiency

For computation energy analysis, we count the total spiking operations (SOPs) to estimate the energy consumption of different distillation SNNs compared with their ANN counterparts (Akopyan et al. 2015). Specifically, we adopt "VGG-11 & ResNet-32x4" combination, then sample 1024 samples and calculate the mean value of SOPs. Early stopping is also used to alleviate overfitting with a tolerance of 20 epochs. We also introduce the direct trained SNN (baseline) for comparison. In conservative estimation, SNNs consume 0.9pJ energy per accumulation (AC) and 4.6pJ energy per multiplication and accumulation (MAC) as measured in 45nm CMOS technology (Rathi and Roy 2021). However, further study proves that the energy consumption of SNNs on specified hardware design can be reduced by 12 \times to 77 fJ/SOP (Rathi and Roy 2021). SNNs in this paper have multiplication operations in the first layer, while the other layers only have addition operations.

Table 3 summaries the results of various SNN training methods with different time steps. Notably, the SNN obtained through SASTC has 79.40% Top-1 test accuracy and 614.1 uJ energy consumption with 2 time steps, which

achieves both the higher performance and higher efficiency compared to directly trained (baseline), vanilla distillation (KD) and feature distillation (feature KD) SNNs with 7 time steps. In addition, the energy is significantly efficient when MAC degrades to AC. For instance, our SASTC trained SNNs outperform the ANN counterpart of 0.18%($T = 2$), 1.02%($T = 3$) and 1.46%($T = 7$) with only 4.91%, 6.73% and 15.71% energy consumption respectively.

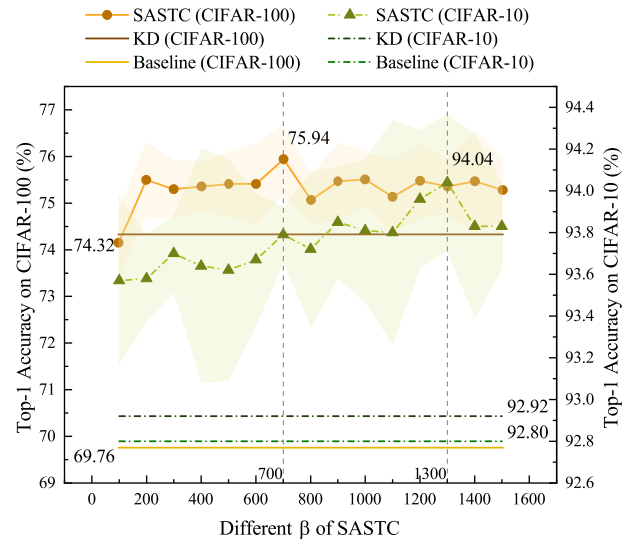


Figure 2: Impact of the hyperparameter β .

Table 3: Comparions of Energy Consumption under Different Time Steps of "ResNet-18 & ResNet-32x4" Combination on CIFAR-100

Method	Time Steps	T=2	T=3	T=7
	Accuracy (%)	70.56	75.72	76.40
Baseline	Total Energy (uJ)	388.3	571.1	1303.9
	Accuracy (%)	77.68	78.00	78.64
KD	Total Energy (uJ)	373.7	560.4	1271.5
	Accuracy (%)	77.2	78.16	78.40
Feature KD	Total Energy (uJ)	378.3	566.3	1259.3
	Accuracy (%)	77.2	78.16	78.40
SASTC	Accuracy (%)	79.40	80.24	80.68
	Total Energy (uJ)	614.1	841.5	1965.6
ANN	Accuracy (%)		79.22	
	Total Energy (uJ)		12511.2	

Note: SNNs adopt three time steps.

Comparison of Running Time and Memory Consumption

We analysis the time and memory cost with the "VGG-11 & ResNet-32x4" combination on CIFAR-100. The overall running time of vanilla ANN-to-SNN KD, feature-based ANN-to-SNN KD and SASTC is about 3.6, 3.0, 2.8 h with 2 time steps, 4.0, 3.2, 3.9 h with 3 time steps, and 6.0, 4.3, 3.6 h

with 7 time steps, respectively. The overall GPU memory usage of these methods is about 0.8 to 1.2 GB based on our training settings and computing infrastructure in Appendix 2. A. Our proposed SASTC obtain similar performance in shorter training time (SASTC with T=2 VS. KD and Feature KD with T=7). While the training time and memory usage vary across methods and ANN-SNN combinations, the comparison results above underscore the superiority of SASTC. Additionally, SASTC requires more computational resources, including time and GPU memory, to achieve its superior performance, which represents an acceptable trade-off.

Experimental Setup

Datasets

- **Static Datasets** focus on popular image classification tasks, including CIFAR-10 (Krizhevsky, Hinton et al. 2009), CIFAR-100 (Krizhevsky, Hinton et al. 2009), and ImageNet (Krizhevsky, Sutskever, and Hinton 2012). Data augmentation is applied on CIFAR-10 and CIFAR-100 by padding each training image with 4 pixels on each side and extracting a randomly sampled 32×32 crop or its horizontal flip. The ImageNet dataset includes over 1.2 million training images, 50,000 validation images, and 100,000 test images across 1,000 classes. For ImageNet, each training image is randomly sampled as a 224×224 crop or its horizontal flip without any padding operation.
- **Neuromorphic Datasets** consist of DVS-Gesture (Amir et al. 2017) and DVS-CIFAR10 (Li et al. 2017) datasets, capturing events reflecting changes in pixel brightness. In the DVS-Gesture dataset, the task involves classifying 2-dimensional event-stream inputs into 11 hand gesture classes. The input event bins are scaled to a 64×64 size before being fed into the model. DVS-CIFAR10 provides each label with 9,000 training samples and 1,000 test samples.

Training Details

We employ the stochastic gradient descent (SGD) optimizer with a momentum of 0.9 in all experiments. For CIFAR-10 and CIFAR-100, the initial learning rate is set to 0.01, and models are trained for 240 epochs with the learning rate divided by 10 at 150, 180, and 210 epochs. The mini-batch size is fixed at 128, and the weight decay is set to 5×10^{-4} . Results are reported as means (standard deviations) over 3 trials. Regarding ImageNet, the initial learning rate is 0.1, reduced by a factor of 10 at 30 and 60 out of the total 90 training epochs. The mini-batch size is set to 256, and the weight decay is 1×10^{-4} , with results reported from a single trial. For consistency and fair comparison, we maintain a temperature α of 4 for the ANN-to-SNN KD loss. For static datasets, the hyper-parameter β of SASTC is set to 1300 on CIFAR-10, 700 on CIFAR-100 and 50 on ImageNet, respectively. For neuromorphic datasets, models are trained using the SGD optimizer for 300 epochs. The initial learning rate is set to 0.1 and divided by 10 at epochs 150, 180, 210, and 260. Additionally, set hyperparameter β to 0.01, 0.1, and 1 at the

first, second, and last 100 epochs, respectively. In practice, the building blocks (i.e., *student layers* and *target layers*) are notably fewer than the total layer count in both SNN and ANN.

Computing Infrastructure

All experiments are conducted using PyTorch (Paszke et al. 2019) on a server equipped with four NVIDIA RTX 3090 GPUs, and another server with four NVIDIA RTX A800 GPUs.

References

- Akopyan, F.; Sawada, J.; Cassidy, A.; Alvarez-Icaza, R.; Arthur, J.; Merolla, P.; Imam, N.; Nakamura, Y.; Datta, P.; Nam, G.-J.; Taba, B.; Beakes, M.; Brezzo, B.; Kuang, J. B.; Manohar, R.; Risk, W. P.; Jackson, B.; and Modha, D. S. 2015. TrueNorth: Design and Tool Flow of a 65 mW 1 Million Neuron Programmable Neurosynaptic Chip. *IEEE Transactions on Computer-Aided Design of Integrated Circuits and Systems*, 34(10): 1537–1557.
- Amir, A.; Taba, B.; Berg, D.; Melano, T.; McKinstry, J.; Di Nolfo, C.; Nayak, T.; Andreopoulos, A.; Garreau, G.; Mendoza, M.; et al. 2017. A low power, fully event-based gesture recognition system. In *Proceedings of the IEEE conference on computer vision and pattern recognition*, 7243–7252.
- Keskar, N. S.; Mudigere, D.; Nocedal, J.; Smelyanskiy, M.; and Tang, P. T. P. 2016. On large-batch training for deep learning: Generalization gap and sharp minima. *arXiv preprint arXiv:1609.04836*.
- Krizhevsky, A.; Hinton, G.; et al. 2009. Learning multiple layers of features from tiny images.
- Krizhevsky, A.; Sutskever, I.; and Hinton, G. E. 2012. Imagenet classification with deep convolutional neural networks. *Advances in neural information processing systems*, 25.
- Li, H.; Liu, H.; Ji, X.; Li, G.; and Shi, L. 2017. Cifar10-dvs: an event-stream dataset for object classification. *Frontiers in neuroscience*, 11: 244131.
- Paszke, A.; Gross, S.; Massa, F.; Lerer, A.; Bradbury, J.; Chanan, G.; Killeen, T.; Lin, Z.; Gimelshein, N.; Antiga, L.; et al. 2019. Pytorch: An imperative style, high-performance deep learning library. *Advances in neural information processing systems*, 32.
- Rathi, N.; and Roy, K. 2021. DIET-SNN: A low-latency spiking neural network with direct input encoding and leakage and threshold optimization. *IEEE Transactions on Neural Networks and Learning Systems*.

Appendix 2

Table 1: Training and Inference Times of Different ANN-to-SNN Distillation Approaches on ImageNet.

Method	Architecture	Time Steps	Training Time (h)	Inference Time (mins)
Baseline	ResNet-18	4	1.34	1.01
KD	ResNet-18	4	1.36	1.01
Feature	ResNet-18	4	1.97	1.12
SASTC (Ours)	ResNet-18	4	2.50	1.07
	ResNet-34	4	4.01	1.93

Table 2: Training and Inference Times per Epoch of Different ANN-to-SNN Distillation Approaches on CIFAR datasets

Model Type	Baseline						KD						Feature KD						SASTC (Ours)								
	T=2			T=3			T=7			ANN (teacher)			T=2			T=3			T=7			T=2			T=3		
	Train	Infer	Train	Infer	Train	Infer	Train	Infer	Train	Infer	Train	Infer	Train	Infer	Train	Infer	Train	Infer	Train	Infer	Train	Infer	Train	Infer	Train	Infer	
CIFAR-10																											
VGG-11	36.77 12.11 37.70 12.46 48.17 12.64						ResNet-19	43.50	19.18	46.50	19.57	62.16	19.84	74.21	10.18	81.42	10.49	120.49	13.88	99.78	13.24	102.24	13.78	117.35	14.99		
	Pyramidnet-20						41.98	19.60	45.11	19.48	60.80	19.57	73.73	10.14	80.26	10.54	135.68	13.07	99.23	13.37	103.36	12.54	123.66	15.40			
	WRN-28-4						41.96	19.57	45.84	19.11	62.29	19.71	97.36	11.56	109.23	11.70	125.93	18.12	100.93	14.60	102.50	13.82	131.22	16.01			
ResNet-18	51.94 12.58 66.34 12.89 71.26 13.02						WRN-28-4	53.26	13.16	68.63	12.69	84.36	12.31	90.95	12.62	105.11	12.40	190.38	13.12	122.67	13.22	161.36	13.03	221.31	12.17		
	Pyramidnet-20						54.35	12.11	67.99	12.76	86.51	12.91	85.68	14.02	90.58	12.99	185.36	13.12	122.87	13.02	160.93	13.47	224.01	11.89			
	WRN-16-2						ResNet-19	100.93	15.22	136.91	14.98	376.60	15.80	114.22	13.78	156.11	13.06	356.33	16.08	171.01	15.12	241.43	15.07	311.81	15.07		
WRN-16-2	Pyramidnet-20						94.75	14.90	132.36	14.78	344.37	15.28	107.43	12.29	152.44	13.11	339.51	16.89	166.14	15.04	233.89	15.32	301.67	15.58			
	WRN-28-4						95.04	14.86	134.35	15.04	359.11	14.86	118.75	12.78	151.44	13.71	328.38	16.13	177.25	15.06	250.11	15.13	306.22	15.29			
CIFAR-100																											
VGG-11	69.21 12.71 73.25 13.12 90.11 13.41						VGG-13	86.77	13.61	90.19	17.44	153.80	18.83	101.22	12.33	125.41	12.91	215.12	12.76	129.99	13.01	130.35	13.53	185.73	13.28		
	ResNet-32x4						90.49	13.89	103.85	18.03	157.44	17.69	108.24	12.75	127.25	12.12	172.49	12.14	108.09	18.41	125.58	13.67	164.58	13.69			
	WRN-40-2						88.67	18.46	103.43	18.45	157.44	18.69	100.89	12.41	124.88	12.76	170.62	13.01	121.88	12.90	125.64	12.74	156.59	13.04			
ResNet-18	ResNet-32x4						88.22	13.58	98.57	18.47	259.07	18.90	91.74	14.06	103.78	14.52	145.46	14.83	114.85	20.03	157.89	20.24	192.65	18.48			
	WRN-40-2						87.99	13.06	99.79	17.00	350.14	17.99	93.12	14.01	101.29	14.17	136.13	15.84	115.23	19.65	157.81	20.32	181.89	18.99			